JOURNAL OF CATALYSIS 87, 414–423 (1984)

EXAFS Study of Zeolite-Supported Rh Catalysts for Methanol Carbonylation

D. R. DENLEY, R. H. RAYMOND, AND S. C. TANG

Shell Development Company, P. O. Box 1380, Westhollow Research Center, M-1250, Houston, Texas 77001

Received August 29, 1983; revised December 22, 1983

In order to determine the structural basis for the activity of transition metals exchanged into zeolite frameworks, a series of extended X-ray absorption fine structure (EXAFS) measurements have been made. In the particular case of Rh, it has been shown that solutions of $[RhCl(NH_3)_5]Cl_2$ exchanged with Na–X form a highly active catalyst ("RhA") for the carbonylation of methanol when used with an organic iodide promoter. On the other hand, systems prepared from $RhCl_3$ are far less active ("RhC"). EXAFS spectroscopy from the Rh K-edge has been used to follow the fate of the Rh species for the two preparation techniques from the initial impregnation through the catalyst calcination to the final activation with the promoter. Differences in structure are readily apparent at each stage of the catalyst preparation. The results indicate that the species present in RhA after impregnation is a mobile aquo complex while the Rh of RhC is in the form of Rh_2O_3 crystallites. Upon calcination, the RhA system forms highly dispersed Rh metallic crystallites while the structure of the Rh species in RhC is only slightly affected by calcination. The activation step in RhA involves modification of the metal particles at the surface atoms in a manner similar to classical metal catalysis. The EXAFS results indicate that the intermediate oxide formed in RhC during calcination is too stable for effective activation since it fails to convert fully to the metal form.

INTRODUCTION

The possible use of Rh catalysts supported by zeolites for the carbonylation of methanol (and related reactions) has attracted substantial attention (*1–5*). This reaction takes place in solution with a CH_3I promoter at moderate temperatures. In the case of the homogenous reaction, the Rh complexes involved form one of the best characterized catalytic systems (*6*). However, far fewer answers are available to the questions that arise regarding the case of the heterogeneous system: (1) Where is the Rh located and what is its neighborhood? (2) What is the valency of Rh? (3) To what extent does Rh maintain its dispersion? and (4) How ac the above points affected by the method of preparation? Infrared spectroscopy and XPS report Rh valencies of the active catalyst that include Rh^0, Rh^I, and more highly oxidized species (*7–11*). However, ir is not a very sensitive probe of cation valence state. At the same time, XPS operates under a disadvantage unique to the zeolite-supported catalysts since the exposed surface external to the catalyst grains is generally only a few percent of the combined external surface and internal surface. Since much of the interest and catalyst design efforts aim at utilizing the high internal surface area of the support and its unusual chemical environment, a method for measuring the chemical structure, valency, etc., in the bulk is most desirable. In the case of the zeolites then, the well-known sensitivity of XPS to the exposed (external) surfaces may act to obscure the chemical state of the majority of the catalytic metal. With this in mind, we have performed measurements of the extended X-ray absorption fine structure (EXAFS) on a series of zeolite-supported Rh catalyst preparations.

The importance of the method of catalyst preparation is well known, but was emphasized in recent work in which Rh is impregnated in NaX zeolite (*5*). In particular, a Rh/NaX catalyst was far more active for

0021-9517/84 $3.00

the carbonylation of methanol when prepared from an aqueous solution of $[Rh(NH_3)_5Cl]Cl_2$ as compared to the more common $RhCl_3$ starting point. In order to obtain an understanding of the structural reasons that might underlie these differences, spectra were taken of systems prepared from solutions of $[Rh(NH_3)_5Cl]Cl_2$ and $RhCl_3$ (which we will refer to as "RhA" and "RhC," respectively).

Experimental

Both RhA and RhC were prepared by impregnation of LINDE 13X from aqueous solutions of the starting compound in the manner described by Christensen and Scurrell (*3*). After washing and drying, the impregnated zeolite samples of the light brown material were reserved for spectroscopy. At this stage of preparation, the material was designated "wet." After calcination at 400°C in flowing N_2, a portion of RhA and RhC were transferred and stored under N_2 for measurements at the "calcined" stage. This material was dark gray for RhA and brown for RhC. The catalyst was then contacted with a mixture of CO, methanol, and methyl iodide at 150°C to produce a catalyst in the working state and is designated the "activated" stage. The analysis of the reaction product showed high selectivity for carbonylation and a high activity for RhA together with a much lower activity for RhC, in agreement with the results of Scurrell and Howe (*5*). These results for two runs are set out in Table 1. The activated catalyst was transferred and stored under N_2. The material RhA became slightly lighter gray upon activation, while the RhC sample was dark brown.

Preliminary to performing spectroscopy on the samples, a sufficient amount of each was loaded into sample holders with a 20-mm-diam barrel bored into either Al or Bn and then capped with BN disks. The holders were then sealed in plastic bags while being maintained under an inert atmosphere. The X-ray absorption measurements in the region of the Rh K-edge (23.2 keV) were made at the C2 station of the Cornell High Energy Synchrotron Source (CHESS). Each experiment involved placing the sample in the X-ray beam and between two ion chambers serving as X-ray detectors. The monochromator stepped the beam through X-ray energies starting at less than the Rh K-edge at 23.21 keV and to energies well above the edge. At each energy the "upstream" detector reports the incident intensity I_0 with little absorption and the detector "downstream" of the sample measures the remaining intensity I. From Beer's law the X-ray optical density $\mu d = \rho(E) = \ln(I_0(E)/I(E))$ is obtained, where d is the sample thickness. Spectral runs required ca. 15 min. Once the spectrum is obtained, the EXAFS is extracted as the oscillatory portion of the absorption spectrum above the absorption edge

$$\chi(E) = \frac{\rho(E) - (\rho_0(E) + \rho_B(E))}{\rho_0(E)}.$$

Here $\rho_0(E) + \rho_B(E)$ is the total background due to the atomic absorption from the edge

TABLE 1

Rh/13X Carbonylation Studies

	CH_3I/CH_3OH molar ratio	Temp (°K)	Rate of carbonylation mole product/g Rh/hr (g product/g Rh/hr)	Selectivity (%)
$RhCl_3$/13X	0.12	423	0.0512 (3.79)	>90
	0.12	423	0.0648 (4.80)	>90
Rh(amine)/13X	0.12	423	0.271 (20.0)	>90
	0.12	423	0.198 (14.3)	>90

being excited, ρ_0, plus all other contributions to the absorption, ρ_B. In this work $\rho_0 + \rho_B$ is empirically obtained as a least-squares fit to the EXAFS region with polynomial spline functions, and ρ_0 is approximated by Heitler's formula (*12*). In order to control possible X-ray induced changes in the samples, rapid scans of the near edge region were made before and after the long EXAFS scan. The lack of a measurable shift in the absorption edge was considered an assurance that radiation damage had not occurred. Also, the samples showed no X-ray-induced color changes during the measurements.

RESULTS AND DISCUSSION

The EXAFS spectra show that the samples underwent important structural changes at each stage of the preparation and that there existed significant differences between RhA and RhC at each stage of preparation. Beginning with the first, "wet" stage, there is an obvious difference in crystallinity. In successive steps the EXAFS amplitude for RhA increases and becomes indicative of high-Z backscattering neighbor-shells, while this transformation lags in RhC.

Rh/13X-Wet

The EXAFS signal χ obtained for RhC-wet and RhA-wet is displayed in Fig. 1 after weighting by a factor k^3 in the electron momentum, together with the radial distribution function (rdf) obtained after a Fourier transform of the EXAFS signal. There is a

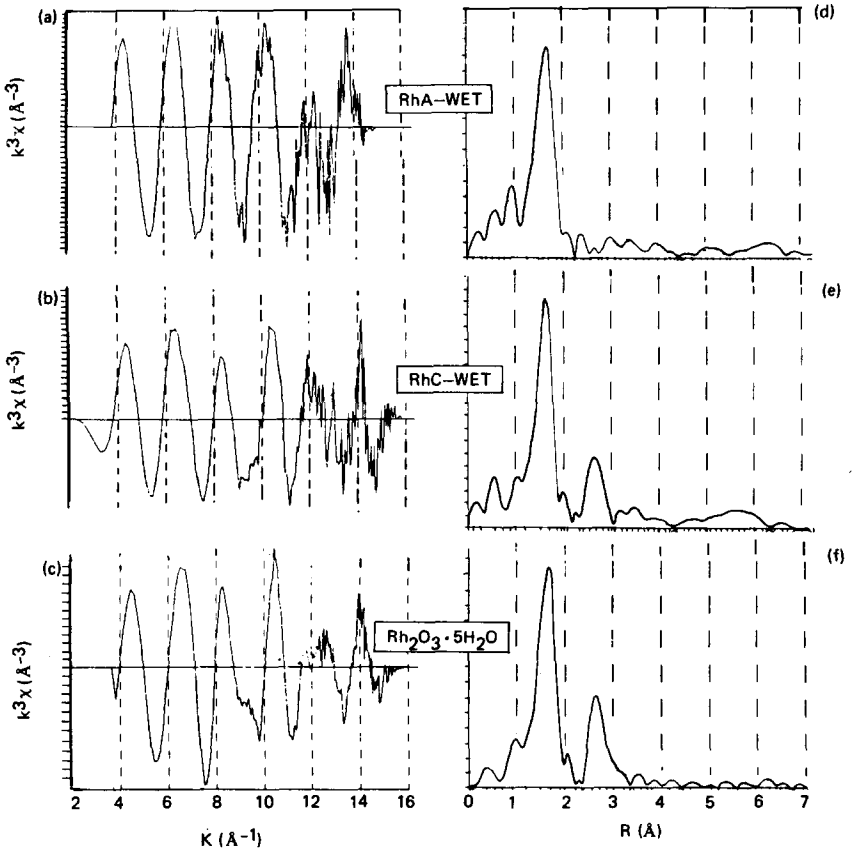

FIG. 1. Rh K-edge EXAFS for (a) RhA catalyst in the "wet" form, (b) RhC catalyst in the "wet" form, and (c) rhodium sesquioxide hydrate. The direct Fourier transforms of these are (d), (e), and (f), respectively.

similarity in the first neighbor-shell in bond distance, but only RhC-wet gives clear evidence of any further neighbor-shells. The rdf for the reference compound Rh_2O_3 hydrate shows striking similarities with RhC-wet and based on the confirmation procedure detailed below, we conclude that RhC-wet is substantially microcrystals of Rh_2O_3 hydrate crystal structure with a Rh atom having O atoms in the first neighbor-shell (abbreviated ns1) at 2.05 Å distance and Rh in ns2 at 3.00 Å. At this point it is worthwhile to outline how the neighbor-shell is identified in our work and how the correct shell distance is determined. Figure 2a shows the EXAFS signal $k^3\chi$ which is then Fourier transformed. The total EXAFS signal is composed of the contribution $\chi_j(k)$ of each of several neighbor-shells which are described by the formula (*13*)

$$\chi_j(k) = (N_j/kR_j^2)|f_j(\pi)| \times \sin[2kR_j + \phi_j(k)] \exp[-2\sigma^2k^2 - 2R_j/\lambda(k)]. \quad (1)$$

The electron wave vector is given by

$$k = 0.5123(\hbar\omega - E_0 + E_i)^{1/2}\ \text{Å}^{-1}, \quad (2)$$

with energies expressed in electron volts, where E_0 is the onset of absorption and the inner potential E_i sets the zero of electron kinetic energy. The total signal is obtained as a sum over shells of jth-neighbor atoms consisting of N_j atoms at a distance R_j from a central atom. The backscattering strength is $|f_j(\pi)|$, and ϕ_j is the total energy-dependent phase shift that an electron experiences upon returning to the central site af-

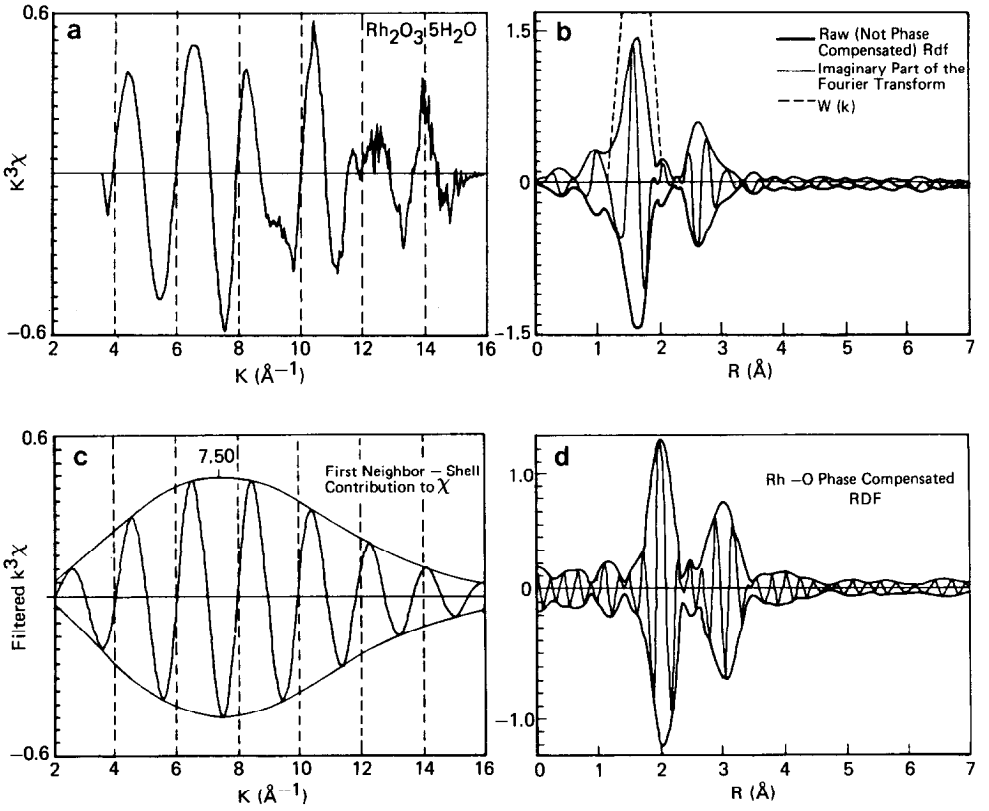

FIG. 2. The analysis used in this work takes (a) the EXAFS signal and applies a Fourier transform to obtain an rdf without phase compensation as in (b). The peak is isolated with a window function [dashed line in (b) and back-transformed to a filtered signal (c)]. After transforming with a phase compensating factor, the rdf in (d) results.

ter backscattering. Thermal oscillations from the equilibrium lattice positions are described by σ, and λ is the mean electron attenuation length. Since χ is a harmonic sum, then a Fourier transform will have the effect of isolating out the contributions to χ of the different shells. The radial distribution function is obtained from the complex Fourier transform $\mathcal{F}(k^n\chi)$ as the absolute value $\mathcal{N}(r) = |\mathcal{F}(k^n\chi)|$ shown in Fig. 2b. The contribution to χ derived from a single neighbor-shell is studied by isolating that shell with a window function $W(r)$ that falls smoothly to zero away from the peak of interest. The isolated peak from shell i is then inverse Fourier transformed to obtain the EXAFS signal from shell i alone $k^n\chi_i = \mathcal{F}^{-1}(W(r)\mathcal{F}(k^n\chi))$ as shown for the primary shell in Fig. 2c. This signal shows a peak which is known to increase in position with atomic number of the neighbor shell atom (*14*). In this way it is possible to assign the approximate atomic number by comparison with similar determinations for compounds of known structure. Table 2 gives values for reference compounds that lead to an identification of the first neighbor shell in RhC-wet as oxygen by comparing with the different k_{max} locations for $k^3\chi$. Finally, in order to obtain the correct values for neighbor distances, it is necessary to take into account the well-known phase lag $\phi(k)$ in χ that has the effect of foreshortened distances in $\mathcal{N}(r)$ by ca. 0.3 Å. This can be quite adequately compensated by multiplying the EXAFS signal by an offsetting phase $e^{-i\phi(k)}$ before Fourier transforming the data (*15*). It can also be helpful to divide out the influence of the backscattering amplitude and the Debye–Waller factors when they are known. In our study we have used phase shifts and amplitudes calculated by Teo and Lee (*14*). The Debye–Waller factors have not been determined here but the k^3 prefactor to χ serves as approximate compensation. The accuracy of this technique is routinely a few hundredths of an angstrom and can be as low as a few thousandths (*15*). This final transformation as shown in Fig. 2d was done on the raw experimental χ, but for cases of close or overlapping shells, it would be more appropriate to act on the filtered data χ_i. In this way transformation of $k^3\chi$ with phase compensation for a Rh absorbing site and an O backscatterer yields an Rh–O first-shell distance of 2.05 Å which agrees very well with a similar EXAFS determination of the Rh–O distance in Rh_2O_3 hydrate of 2.04 Å. By a similar process we can confirm the second largest peak as being due to Rh atoms in ns2 at a distance of 3.00 Å. The good agreement of this distance with the ns2 of Rh_2O_3 hy-

TABLE 2

Rh K-EXAFS; Reference Compounds

Sample	Peak in Fourier transform (Å)	Max in $k^3\chi$ (Å^{-1})	Bond
RhI_3	2.38	10.9	Rh–I
Rh(m)	2.38	10.6	Rh–Rh
$RhCl_3$/anh	1.87	8.6	Rh–Cl
$Rh_2O_3 \cdot 5H_2O$	1.62	7.5	Rh–O
$RhCl(NH_3)_5Cl_2$	1.64	7.1	Rh–N

TABLE 3

Rh K-EXAFS: Phase Compensated Neighbor-Shell Distances in Reference Compounds

Sample	Bond	EXAFS distance (Å)	XRD value (Å)	Sum of Bragg–Slater atomic radii[a] (Å)
RhI_3	Rh–I	2.65	2.63[b]	2.75
Rh(metal)	Rh–Rh	2.68	2.69[c]	2.70
	Rh–Rh	3.84	3.80[c]	
	Rh–Rh	4.65	4.66[c]	
$RhCl_3$ anhydrous	Rh–Cl	2.30	2.30[d]	2.35
$Rh_2O_3 \cdot 5H_2O$	Rh–O	2.04		1.95
	Rh–Rh	3.04		
$RhCl(NH_3)_5Cl_2$	Rh–N	2.05	2.06[e]	2.00

[a] Day, C., and Selbin, J., "Theoretical Inorganic Chemistry," p. 114. Reinhold, New York, 1965.

[b] Denley, D., unpublished data.

[c] Wyckoff, R. W., "Crystal Structures," Vol. 1, p. 79. Wiley–Interscience, New York, 1963.

[d] Griffith, W. P., "The Chemistry of the Rarer Platinum Metals," p. 40. Wiley–Interscience, London, 1967.

[e] Evans, R. S., Hopcus, E. A., Bordner, J., and Schreiner, A. F., *J. Cryst. Mol. Struct.* **3**, 235 (1973).

drate (Table 3), the excellent agreement for ns1, and the correspondence of the relative peak amplitude serve as strong evidence for the identification of RhC-wet with microcrystalline Rh_2O_3 hydrate.

Just as with RhC, the location of k_{max} for the primary peak of RhA-wet indicates an oxygen first neighbor. The obvious difference in RhA-wet from RhC-wet and Rh_2O_3 hydrate is the absence of the Rh–Rh second neighbor-shell. The RhA-wet also does not appear to be bound at one of the traditional cation sites of faujasite as evidenced by the absence of Al or Si neighbor-shells. In fact, the complete absence of higher neighbor-shells indicates that the Rh is in the form of a mobile, mononuclear aquo complex. However, because of the close value of k_{max} for N in comparison to that of O and the similar value for Rh–N as found by EXAFS and XRD (*16*) for $[RhCl(NH_3)_5]Cl_2$ (Table 3), it is difficult to rule out the possibility of the first neighbor as being N (presumably as an ammine coordination sphere).

Rh/13X-Calcined

The differences between RhA and RhC become more pronounced at the calcined stage (Fig. 3). The RhC-calcined results show a Rh–O ns at 2.02 Å and a Rh–Rh ns at 2.98 Å. These results are once again consistent with Rh_2O_3 hydrate type of structure in both shell distances and amplitudes. The small shell shrinkage observed in going from RhC-wet and Rh–C calcined could be the Rh_2O_3 crystallite responding to internal pressure generated by dehydration of the hydrate lattice.

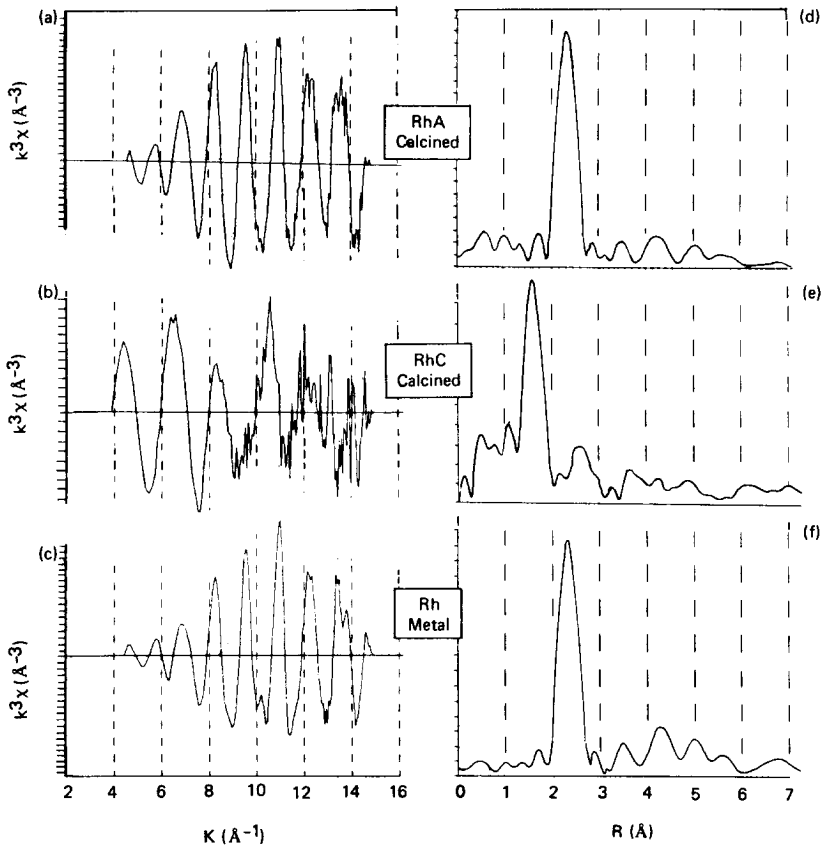

FIG. 3. Rh K-edge EXAFS for (a) RhA catalyst at the calcined stage, (b) RhC catalyst at the calcined stage, and (c) Rh metal. The direct Fourier transforms of these are (d), (e), and (f), respectively.

TABLE 4

Rh/13X EXAFS Bond Distances

Sample	Bond	Max in $k^3\chi$ (Å^{-1})	Distance (Å)
RhA-wet	Rh–O	7.8	2.06
RhA-calcined	Rh–Rh	10.3	2.67
	Rh–Rh		3.84
	Rh–Rh		4.59
RhA-activated	Rh–Rh	10.5	2.63
	Rh–Rh		3.74
	Rh–Rh		4.51
RhC-wet	Rh–O	7.7	2.05
	Rh–Rh	10.0	3.00
RhC-calcined	Rh–O	7.5	2.02
	Rh–Rh	10.1	2.98
RhC-activated	Rh–O	7.0	1.95
	Rh–Rh	10.2	2.69

The RhA-calcined material (Fig. 3) is readily identified by EXAFS as Rh metal crystallites. Upon comparison of the results in Tables 3 and 4, the apparent bond contraction and the decreased intensity of higher neighbor-shells are both consistent with the Rh being in the form of very small crystallites (*17*).

Attempts to locate Rh or measure crystal size by XRD proved fruitless so an estimate of the crystal size from the EXAFS data was made. The neighbor-shell peak function $\mathcal{N}_j(r)$ obtained by Fourier transforming χ_j in Eq. (1) has its main dependence in overall amplitude on N_j/R_j^2. Then it is possible to obtain an estimate of the fractional change f_j in N_j of the crystallites from that of the chemically identical reference metal in the form of a bulk powder if the simplifications are made that one can neglect effects due to changes in the electron phase and backscattering function, Debye–Waller factor, inelastic attenuation or the level of static disorder,

$$f_j = \frac{N_j}{N_j^{\text{ref}}} = \frac{R_j^2}{(R_j^{\text{ref}})^2}\frac{P_j}{P_j^{\text{ref}}},$$

where P_j is the peak amplitude of the jth shell in the rdf. Since the variations in R_j and overall chemical environment between the reference material (bulk metal) and the sample (microcrystallites) are so small, the effect of the approximations made are expected to be small in this case.

The values of f_1 and f_2 for RhA-calcined using Rh foil as a reference are 0.49 and 0.34. These can be compared to the values obtained from model calculations for small

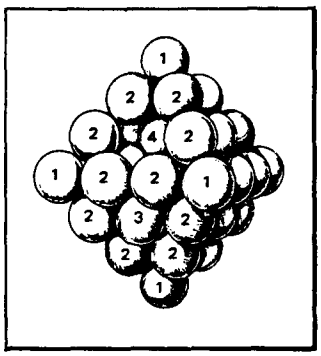

Population

Four Types of Atoms with Differing Occupancies of The Neighbor – Shells

Atom Type Number	Occupancy of Neighbors in: ns 1	ns 2
1 Corner	4	1
2 Edge	7	2
3 Face	9	3
4 Internal	12	6

$n_c = 6$

$n_e = 12L$

$n_f = 4L(L-1)$

$n_i = \frac{1}{3}L(L-1)(2L-1) + L^2$

L = Total Number of Type 2 Atoms (Along Edge but Not on a Corner)

FIG. 4. Summary of the attributes of an octahedral model arising from a face-centered cubic lattice.

TABLE 5

Octahedron Model: Effect of Size

Total edge length $L_T = L + 2$	Total atoms	n_e	n_f	n_i	Mean occupancy S_L			
					S_L(ns1)	S_L(ns2)	$\frac{S_L(ns1)}{S_\infty(ns1)}$	$\frac{S_L(ns2)}{S_\infty(ns2)}$
2	6	0	0	0	4	1	0.33	0.17
3	19	12	0	1	6.32	1.82	0.53	0.30
4	44	24	8	6	7.64	2.59	0.64	0.43
5	85	36	24	19	8.47	3.11	0.71	0.52
10	670	96	224	344	10.21	4.38	0.85	0.73
20	5340	216	1224	3894	11.10	5.14	0.93	0.86
∞	—	—	—	—	12	6	—	—

crystallites. We have computed theoretical values of the above ratios from the mean ns1 and ns2 occupancies S_L for an octahedron model of the microcrystallite. This model, and its properties as a function of crystallite size, is illustrated in Fig. 4. The resulting values for integral values of the number of atoms along an edge are given in Table 5. The agreement between $S_L(ns1)/S_\infty(ns1)$ and N_1' on the one hand, and $S_L(ns2)/S_\infty(ns2)$ and N_2' on the other is good for an octahedron with a total of ca. 3 atoms along a side. More accurate solutions are shown in Table 6. The quality of the agreement is quite encouraging and could be improved further by modifying the model crystallite to the form of a truncated octahedron.

Rh/13X-Activated

The differences between RhA and RhC in the activated stage suggest the cause of the relatively poor performance of RhC. Two major peaks occur in the spectrum for RhC-activated shown in Fig. 5, the first is at a distance that suggests an Rh–O bond still remains in the nearest neighbor-shell. The position of the peak in the amplitude for χ tends to confirm this, although interference from the stronger peak creates difficulty in confirming this assignment. The peak at 2.69 Å is readily identified as being due to Rh–Rh. Unlike rhodium sesquioxide (Rh–Rh distance of 3.04 Å), the bond length is found to be the closest packing value as in Rh metal, and this, together with comparison to the RhC-calcined spectra, leads us to conclude that Rh–C-activated material actually consists of a mixture of Rh metal crystallites and rhodium oxide in the same form as RhC-calcined. The lack of any bond contraction in the Rh–Rh peak also implies the Rh crystallites are relatively large.

TABLE 6

Rh Crystallite Sizes Derived from the Octahedron Model

Sample	f_1	f_2	Mean crystal size	
			$L_T(f_1)$	$L_T(f_2)$
RhA-calcined	0.49	0.34	2.8	3.2
RhA-activated	0.48	0.43	2.7	4.0

The RhA-activated spectra (Fig. 5) shows very little change from the calcined stage. Since the peak positions (Table 4) and the relative amplitudes are quite similar to the latter, we conclude that the form is nearly the same. The presence of CH_3I as a catalytic promoter, the small shift of the backtransformed amplitude peak toward higher k, and the involvement of I with Rh as a ligand in the case of the homogeneous

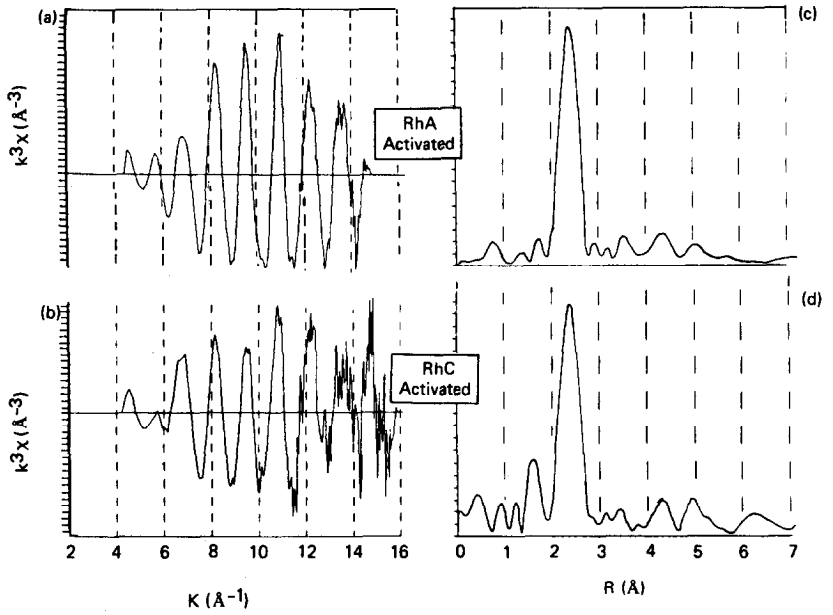

FIG. 5. Rh K-edge EXAFS for (a) RhA catalyst in the activated form and (b) RhC catalyst in the activated form. The direct Fourier transforms of these are (c) and (d), respectively.

process (*6*) create the belief that I ligands have some involvement with the Rh crystallites at the RhA-activated stage. However, this involvement is minor (perhaps decorating the surface of the Rh crystallite) and cannot be confirmed. The estimated size of the crystallite as obtained from the octahedron model (Table 6) is quite similar to that of the calcined stage.

CONCLUSION

This EXAFS study was aimed at trying to understand the structural differences between a highly active and a low activity formulation of a Rh/13X catalyst for methanol carbonylation. Structural differences were in fact found at the earliest preparation stage. Since no Rh–N interaction could be demonstrated for RhA and likewise for Rh–Cl in RhC, it is judged that the initial ligands are not involved directly in the catalyst preparation beyond the initial stage of Rh impregnation into the zeolite lattice. In the impregnated stage, RhA-wet is most likely in the form of a highly dispersed oxide or aquo complex. The lack of secondary neighbor-shells indicates either high static disorder or perhaps cationic mobility. The RhC-wet sample shows very strong similarity to bulk $Rh_2O_3 \cdot 5H_2O$. The RhC-calcined material is not greatly changed aside from some bond contraction that could be due to pressure from the zeolite lattice or perhaps thermal damage to the oxide hydrate. At the same time, RhA-calcined has undergone a dramatic decomposition to Rh metal microcrystallites. This form of RhA does not change substantially upon activation and suggests that a view of catalytic activity as arising from a near homogeneous catalytic process fixed within the "solid solution" of the zeolite framework would be somewhat inaccurate. Instead, the zeolite should be viewed as an unusual carrier of high surface area for metal–particle heterogeneous catalysis. The particle size in both RhA-calcined and activated are similar and estimated at an average of ca. 9 Å, which is quite similar to the main cavity size of the faujasites of ca. 12 Å. The pattern of a RhC carrying a relatively inert Rh species continues into the preparation of RhC-activated, which seems

to show only partial conversion from the oxide to active metal.

ACKNOWLEDGMENT

Two of the authors (D.R.D. and R.H.R.) thank the staff of the Cornell High Energy Synchrotron Source for their cooperation.

REFERENCES

1. Yashima, T., Ebisawa, M., and Hara, N., *Chem. Lett.* **6,** 473 (1972).
2. Yashima, T., Ebisawa, M., and Hara, N., *J. Catal.* **36,** 320 (1975).
3. Christensen, B., and Scurrell, M. S., *J. Chem. Soc. Faraday Trans. I* **74,** 2313 (1978).
4. Essler, E., Queck, S., Koegler, H., and Wendt, G., German (East) Patent No. 129269, 1978.
5. Scurrell, M. S., and Howe, R. F., *J. Mol. Catal.* **7,** 535 (1980).
6. Roth, J. F., Craddock, J. H., Hershman, A., and Paulik, F. E., *Chemtech* 600 (October 1971); Forster, D. J., *J. Amer. Chem. Soc.* **98,** 846 (1976).
7. Yamanis, J., and Yang, K-C., *J. Catal.* **69,** 498 (1981).
8. Okamoto, Y., Nobumasa, I., Toshinobu, I., and Teranishi, S., *J. Catal.* **58,** (1979).
9. Kuznicki, S. M., Eyring, E. M., *J. Catal.* **65,** 227 (1980).
10. Andersson, S. L. T., and Scurrell, M. S., *J. Catal.* **59,** 356 (1979).
11. Primet, M., Vedrine, J. C., and Naccache, C., *J. Mol. Catal.* **4,** 411 (1978).
12. Lengeler, B., and Eisenberger, P., *Phys. Rev.* **B21,** 4507 (1980).
13. Lytle, F. W., Sayers, D. E., and Stern, E. A., *Phys. Rev.* **B11,** 4825 (1975).
14. Teo, B-K., and Lee, P. A., *J. Amer. Chem. Soc.* **101,** 2815 (1979).
15. Lee, P. A., and Beni, G., *Phys. Rev.* **B15,** 2862 (1977).
16. Evans, R. S., Hopcus, E. A., Bordner, J., and Schreiner, A. F., *J. Cryst. Mol. Struct.* **3,** 235 (1973).
17. Apai, G., Hamilton, J. F., Stohr, J., and Thompson, A., *Phys. Rev. Lett.* **43,** 165 (1979).